Research on Chemical Intermediates
https://doi.org/10.1007/s11164-020-04255-z

Carbon dioxide conversion into the reaction intermediate sodium formate for the synthesis of formic acid

Muhammad Hanan Masood[1] · Noor Haleem[1] · Iqra Shakeel[1,2] · Yousuf Jamal[1]

Received: 9 April 2020 / Accepted: 20 August 2020

Abstract

Increased carbon dioxide (CO_2) emissions from anthropogenic activities are a contributing factor to the growing global warming worldwide. The economical method to recover and effectively reuse CO_2 is through adsorption and absorption. In this study, CO_2 is absorbed into the solution of sodium hydroxide having various concentrations (0.01, 0.1, 0.5, 1.0, 3.0 and 5.0 N), and the impact of the solution pH on the various product formation was observed. The resultant products formed at different pH of the absorbing solution are sodium carbonate at pH 10, Trona at pH 9, and sodium hydrogen carbonate at pH 8. The products formed are confirmed through X-ray diffraction analysis. After pH optimization, the sodium hydrogen carbonate formed at pH 8 is converted into sodium formate through hydrogenation in the presence of nickel ferrite catalyst at 80 °C and atmospheric pressure. The sodium formate produced is then used as a precursor to synthesize formic acid upon simple reaction with sulfuric acid. A reaction % age yield of $79 \pm 0.2\%$ formic acid is noted. Condensed formic acid vapors are later analyzed, using a high performance liquid chromatography for the qualitative analysis.

Keywords Carbon dioxide absorption · Sodium carbonate · Sodium hydrogen carbonate · Sodium formate · Nickel ferrite · Formic acid

✉ Yousuf Jamal
yousuf.jamal@iese.nust.edu.pk

[1] Institute of Environmental Sciences and Engineering (IESE), School of Civil and Environmental Engineering (SCEE), National University of Sciences and Technology (NUST), Sector H-12, Islamabad 44000, Pakistan

[2] School of Chemical and Materials Engineering (SCME), National University of Sciences and Technology (NUST), Sector H-12, Islamabad 44000, Pakistan

Published online: 31 August 2020

Introduction

CO_2 from industrial, transportation and other anthropogenic activities is increasing all over the world causing global warming. CO_2 in the atmosphere, mostly comes from the generation of electricity from coal, furnace oil, diesel and gasoline burning at industries along with biomass burning by humans [1]. CO_2 is one of the greenhouse gases and is a major concern to the environment. With the increase in population and modernization in lifestyle, energy demand is continually increasing. To meet these energy demands, many industrial processes are carried out on a daily basis [2, 3]. The reported threshold concentration of carbon dioxide in the atmosphere is 350 ppm [4], but due to an increase in energy generation, this value is increasing daily. It has been reported that between 1880 and 2012, the overall average temperature of the globe has increased by 0.85° C [5]. Furthermore, carbon dioxide gas emissions are affecting human life on earth in the form of irregular weather patterns, polar ice caps depletion and glaciers melting [6]. In order to reduce the carbon dioxide concentration of the open atmosphere, several separation techniques have been opted [7]. Removed CO_2 can also be recycled and reused to produce various fuels or chemicals [8, 9]. The commercially utilized carbon dioxide separation techniques are the CO_2 adsorption on a solid catalyst surface [10], absorption in the chemical solvents [11] and ionic liquids [12]. The primary advantage of practicing absorption technique over a large scale is that the utilized solvent chemical can be rejuvenated by the simple heating at high temperatures and/or by depressing the system pressures.

Normally, the absorption of CO_2 at source in industries is done by amine scrubbing with chemicals like alkanolamines [13]. Various types of amines that can be used for absorption are: primary amine or monoethanolamine (MEA), secondary amine or diethanolamine (DEA), tertiary amine or N-methyl diethanolamine (MDEA), cyclic amine piperazine (PZ) and sterically hindered amines like 2-amino-2-methyl-1-propanol (AMP) [14]. Alkali metal solutions have also shown promising trades in the carbon dioxide absorption process. Some of the benefits of alkali solutions are the multi-reaction by-product formation [15, 16], whereas there are no reaction products are produced in the case of CO_2 absorption in the amine solutions [17], thus resulting in no value added by reaction products.

During the process of carbon dioxide gas absorption, phase transformation over a heterogeneous catalyst has also been reported to reduce its concentration in the industrial exhausts. Christopher et al. [18] have shown carbon dioxide transformation into organic compounds by intermolecular transfer of hydrogen from metallic hydrogen carbonate solutions, using complex catalysts. Hydrogenation is an endothermic process that requires high reaction temperatures. Many expensive catalysts are reported for use in the hydrogenation process like palladium (Pd), ruthenium (Ru) and rhenium (Re). The presence of these catalysts reduces the reaction temperatures.

Nickel (Ni) has gained importance for the CO_2 reduction in various chemicals at low temperatures [19]. It is most abundant and inexpensive metal. Due to high activity and high surfaces-to-volume ratio and its nontoxic characteristic,

nickel has been used in the hydrogenation reactions. Nickel-based nanoparticles facilitate the reactions in the production of formates. Due to these characteristics, nickel has become the preferred option to use as a metal catalyst [20]. Chen et al. [21] have reported the synthesis of organic acids by the reduction of sodium hydrogen carbonate using Ni powder catalyst supported with hydrazine monohydrate ($N_2H_4{\cdot}H_2O$), as a reductant and reported a 50% reaction yield of formic acid at 300° C. Wang et al. [22] has studied the hydrogenation of carbonate solutions by using a nonporous Ni catalyst and have reported 86.6% yield of formic acid from sodium hydrogen carbonate ($NaHCO_3$) at 200° C. Chiang et al. [23] have studied the hydrogenation of CO_2 over the $Cu/ZnO/Al_2O_3$ catalysts at 30 bar pressure while keeping the H_2/CO_2 mixture ratio (1:1) at 40° C. They reported only 7.6% reaction yield of formic acid. Zhao et al. [24] performed experiments for formic acid synthesis by using sodium carbonate (Na_2CO_3) as an additive and rhodium phosphine complex [RhCl $(mtppms)_3$] as a catalyst and attained 35% yield of formic acid at 50° C. Formic acid has multiple uses in hydrogen storage and production and the released hydrogen conversion into several chemicals [25]. Formic acid can be used as acidifiers for animal feeds and hydrogen source material for several alcohols, amines and alkynes [26].

Based on the literature review, the objective of this research work is to (1) synthesize the reaction products of CO_2 gas absorption into the sodium hydroxide solution of different concentrations and pH, while keeping the absorption temperature low; (2) synthesize the formic acid by the conversion of absorption reaction product sodium hydrogen carbonate into an intermediate reaction product sodium formate, in the presence of nickel ferrite heterogeneous catalyst, followed by the reaction of sodium formate with sulfuric acid and the condensation of the formic acid vapors.

Experimental details

Materials

In order to conduct the experiments, following chemicals were used: sodium hydroxide, NaOH, 99.0% pure (Merck), iron nitrate, $Fe(NO_3)_3$, 98% pure (Merck), nickel nitrate, $Ni(NO_3)_2$, 98% pure (Sigma Aldrich), and Sulfuric acid H_2SO_4, 98% pure (Sigma Aldrich); carbon dioxide (CO_2) gas cylinder with 99% purity (Pakistan Pure Gases Company); and pure zinc metal (Biocare Scientific Company, Pakistan). All chemicals were utilized as received without any further purification.

Batch CO_2 absorption reactions

For CO_2 absorption, six concentrations of sodium hydroxide aqueous solution (0.01, 0.1, 0.5, 1.0, 3.0 and 5.0 N) were prepared by dissolving NaOH pellets into 500 mL of distilled water. The experimental setup is shown in Fig. 1. The temperature of the CO_2 absorbing sodium hydroxide solution was maintained at room temperature (25° C). The CO_2 gas was bubbled through the solution

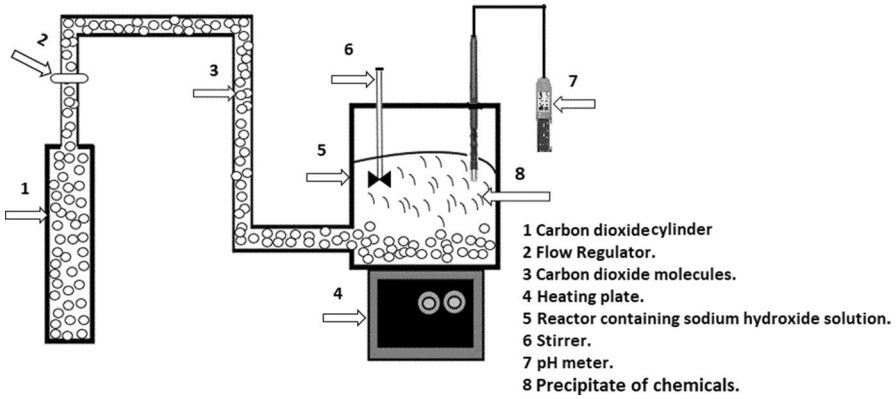

Fig. 1 Experimental setup for CO_2 absorption

[27] at a flow rate of 0.4 L/min, and the pH of the system was monitored for the whole period of the absorption by keeping electronic pH meter in the solution. CO_2 was absorbed in the solution until the final solution pH dropped to 10, 9 and 8 from the starting pH of the sodium hydroxide solution. The total absorption time was also noted. In all the experimental work, a new CO_2 absorbed solution was prepared for reaching the final desired pH of the solution. Absorption solutions were prepared from pH 10 to pH 8 to find out the optimum pH at which maximum sodium hydrogen carbonate is produced. Once the solution pH reduced to the desired pH, the flow of CO_2 was stopped and the reacted solution was oven-dried at 105° C for 24 h and weight of the product obtained at the respective pH was noted down.

X-ray diffraction (XRD, D8 Advance Germany) of the product crystals was performed to analyze the type of the product formed at each solution final pH. The XRD pattern obtained was then analyzed and compared using the MDI Jade 5.0 software. The XRD peaks were matched with the reference peaks.

Synthesis of nickel ferrite catalyst

The nickel ferrite ($NiFe_2O_4$) catalyst for the reaction was produced by mixing a solution of nickel nitrate (0.24 g/mL) and iron nitrate (0.12 g/mL). The two solutions were mixed thoroughly in a beaker while stirring at 100 rpm. The mixture pH was adjusted at pH 12 by adding 1 N sodium hydroxide solution drop by drop. Mixing proceeded at 80° C for 3 h, and the reaction mixture was then allowed to settle down overnight. A mixture paste was formed that was washed with distilled water until pH 7 was achieved. It was then oven-dried at the 110° C for 24 h. The dried crystals produced were placed in a muffle furnace for 6 h at 850° C. Produced nickel ferrite was then analyzed by XRD and scanning electron microscope (SEM, VGA 3, China) analyzer.

Catalytic conversion of sodium hydrogen carbonate to sodium formate through hydrogenation in the presence of nickel ferrite catalyst

To produce the sodium formate ($NaHCO_2$) from sodium hydrogen carbonate ($NaHCO_3$), the reaction was carried out in a reactor attached with a round bottom flask. Hydrogen gas was produced in the flask by the reaction of zinc metal rings with sulfuric acid. Sodium hydrogen carbonate (100 mL, 1 M) was put into the reactor. Two hundred milligrams of nickel ferrite catalyst was introduced into the reactor; then, the hydrogen gas was bubbled into the sodium hydrogen carbonate solution for 2 h at a temperature of 80° C and at the atmospheric pressure. The solution was stirred at 100 rpm, and after the completion of the reaction, the left solution was evaporated at 105° C for 24 h to obtain the sodium formate attached over the nickel ferrite catalyst surface. This material was then stored in air tight bags until further use.

Synthesis of formic acid

For the synthesis of formic acid, 5 g of sodium formate material produced in the hydrogenation reaction of sodium hydrogen carbonate in the presence of nickel ferrite catalyst was converted into formic acid by reacting it with 5 mL of the sulfuric acid. The sulfuric acid was added to dissolve out all of the sodium formate from the nickel ferrite catalyst surface. The formic acid and sodium sulfate were obtained as the reaction product and byproduct, respectively. The vapors of formic acid were condensed to get formic acid in the liquid phase. The sodium sulfate solids from the reaction mixture were made dissolved in water and dried in the oven at 100 ± 5° C for 24 h. Sodium sulfate and formic acid were then analyzed by XRD and high-performance liquid chromatography (HPLC), respectively, having a column of C-18 Merck, UV detector and a mobile phase (buffer + methanol, 95:5) solution, keeping a flow rate of 1 mL/min. (HPLC model: Agilent 1100 series).

Results and discussion

Absorption mechanism of CO_2 in sodium hydroxide solution

Carbon dioxide absorption in sodium hydroxide solution is explained by the following mechanism [28–30]. When the sodium hydroxide solution is prepared, it easily dissociates into Na^+ ions and OH^- ions. As CO_2 is passed through the sodium hydroxide solution, it is physically transformed into the aqueous phase as shown in Eq. 1.

$$CO_2(g) \rightarrow CO_2(aq) \tag{1}$$

As the carbon dioxide absorbs in the sodium hydroxide solution, it reacts with the OH^- ions and form HCO_3^- ions as shown in Eq. 2.

$$CO_2(aq) + OH^-(aq) \rightleftharpoons HCO_3^-(aq) \tag{2}$$

HCO_3^- ions formed further react with OH^- ions and convert into CO_3^{-2} ions as shown in Eq. 3.

$$HCO_3^-(aq) + OH^-(aq) \rightleftharpoons H_2O(I) + CO_3^{-2}(aq) \tag{3}$$

Equations (2) and (3) are highly reversible reactions.

Equation (3) is more dominant than Eq. (2). As the absorption reaction proceeds toward pH 10, depletion of HCO_3^- ions occur in the solution and more CO_3^{-2} ions are formed. These CO_3^{-2} ions react with Na^+ ions and form the Na_2CO_3 product. The overall reaction is shown in Eq. 4:

$$2NaOH(aq) + CO_2(g) \rightarrow Na_2CO_3(aq) + H_2O(I) \tag{4}$$

$pH = 10$.

Considering Eq. (3), for a solution with pH < 10, the backward reaction dominates with more HCO_3^- ions formed in the solution. At pH > 10, the forward reaction dominates with the greater production of CO_3^{-2} ions in the solution.

As more carbon dioxide is fed into the solution, the Na_2CO_3 formed in the solution reacts more with the CO_2 and converts into $NaHCO_3$ as shown in Eq. 5.

$$Na_2CO_3 + H_2O + CO_2 \rightarrow 2NaHCO_3 \tag{5}$$

$pH = 8$.

In this way, more amount of $NaHCO_3$ is produced at pH < 10 and maximum at $pH = 8$.

Impact of sodium hydroxide solution concentration on absorption time

Figure 2 interprets the results of CO2 absorption in sodium hydroxide solution until the starting pH of the solution is dropped to pH 9. The minimum time to reach pH 9 was 3 min in the solution concentration of 0.01 N and was 17 h and 68 h for 3 N and 5 N sodium hydroxide solution, respectively. This is due to the fact that increasing the sodium hydroxide solution concentration increases the concentration of Na^+ and OH^- ions in the solution, which increases the time for their neutralization. This results in the further absorption of CO_2 gas in the solution due to which time to achieve the desired pH increases [28, 31, 32].

It was further noted in Fig. 3 that a minimum of 381 mg of product crystals was obtained at 0.01 N solution, while 65,000 mg and 121,000 mg were measured for 3 N and 5 N sodium hydroxide solution, respectively, when the solution's initial pH was dropped to pH 9 by carbon dioxide absorption. Minimum alkalinity was noted for 0.01 N solution was 24 mg/L equivalent of $CaCO_3$, and maximum alkalinity was 38,000 mg/L and 67,000 mg/L equivalent of $CaCO_3$ for 3 N and 5 N solution, respectively. This increase in alkalinity shows the increasing reaction of the CO_2

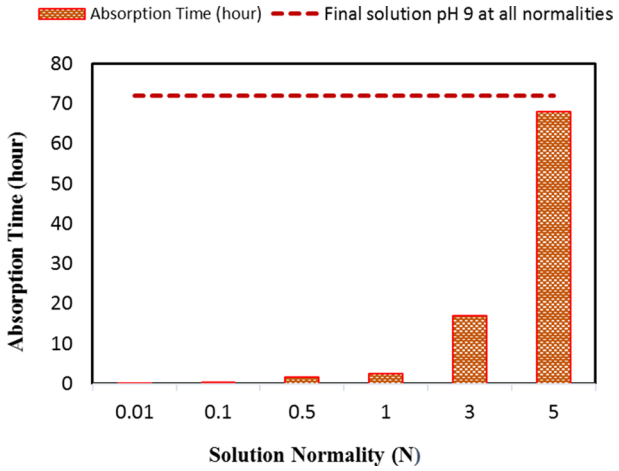

Fig. 2 Impact of solution concentration on absorption time to reach $pH = 9$

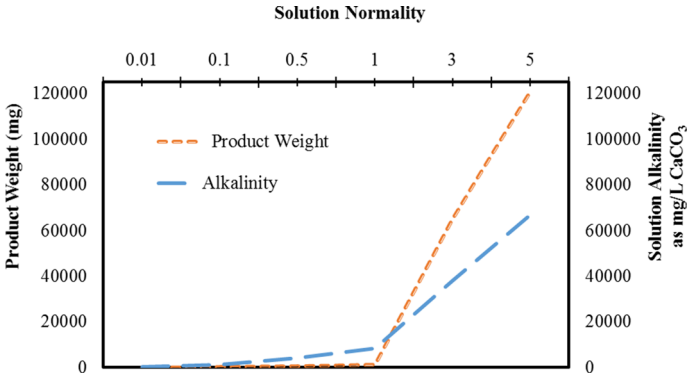

Fig. 3 Impact of solution normality on product formation and solution alkalinity

absorption with the strength of sodium hydroxide solution. Furthermore, it can be said that the minimum sodium hydroxide solution normality required for product formation by the absorption of CO_2 should be above 1 N. Above this solution normality, the alkalinity of the solution suppresses while the amount of product formed increases.

XRD analysis of products formed at different solution pH

XRD analysis of the crystals produced in 3 N solution at pH 9 is shown in Fig. 4, confirming the formation of the reaction product Trona, having a chemical formula of $Na_2CO_3.NaHCO_3.2H_2O$. The XRD analysis showed major peaks presence at 2θ, 18.3°, 29.2°, 33.9° and 44.8° which correspond to the planes (400), (211), (411) and (802). On software analysis, all peaks showed the presence of the same product

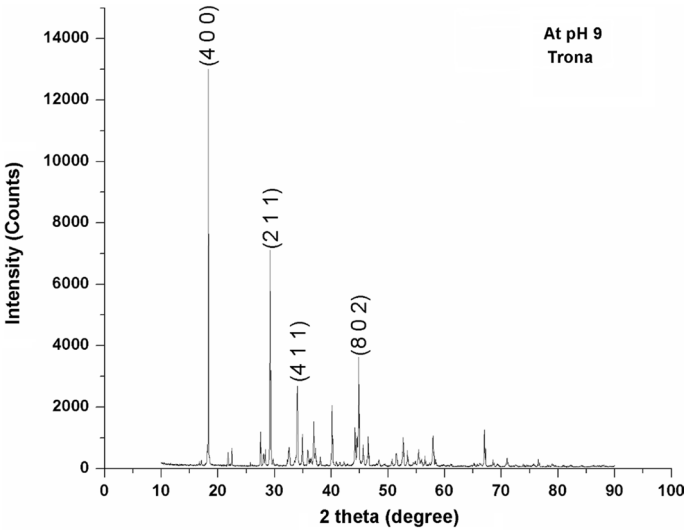

Fig. 4 XRD analysis of Trona

Trona [28]. Trona has multiple uses like in the glass, cement manufacturing industries, and as an animal feed additive for the dairy industry; also it finds an application for the removal of acid gases like oxides of sulfur from flue gases and as a source for soda ash manufacturing industries. Figure 5 shows the XRD analysis of product crystals formed at solution pH 8 and shows the presence of pure sodium

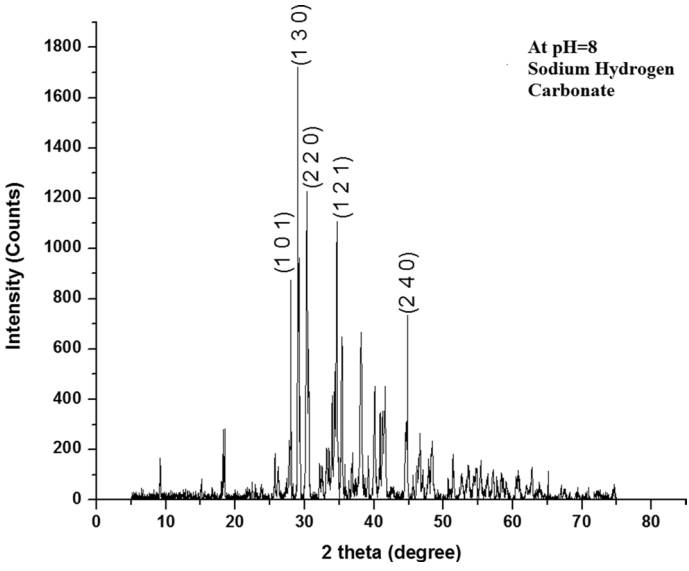

Fig. 5 XRD analysis of sodium hydrogen carbonate

hydrogen carbonate. Major peaks were present at 2θ, 27.70°, 29.0°, 30.2°, 34.6° and 44.7° which attribute to the plane (101), (130), (220), (121) and (240), respectively. Similarly, XRD analysis of the crystals obtained at pH 10 is shown in Fig. 6. It has revealed the presence of pure sodium carbonate crystals. Sharp peaks were prominent at 2θ, 30.0°, 34.3°, 37.8° and 41.3° which match to the plane (002), (310), (112) and (400), respectively. This reveals that the solution pH has a major effect on the type of the product formed.

Impact of solution pH on the weight of absorption products formed

In the 3 N sodium hydroxide solution, the weight of sodium hydrogen carbonate crystals formed were higher than that of sodium carbonates, i.e., 76.6 g and 20.6 g at pH 8 and pH 10, respectively. While the weight of Trona crystals formed was 65.0 g under the presence of same reactants, sodium hydroxide solution and carbon dioxide, at pH 9.

Impact of CO_2 absorption on sodium hydroxide solution exhaustion time

Results showed different exhaustion times at different pH when carbon dioxide was absorbed in the 3 N sodium hydroxide solution. The starting 3 N solution pH was 13.75. The exhaustion time to reach a new solution pH was of the order: pH13 < pH12 < pH11 up to.

pH 8 as shown in Fig. 7.

The higher CO_2 reaction rate is observed at higher solution pH where the concentration of Na^+ and OH^- ions in the solution is also high while the reaction rate becomes slower at low solution pH values [28, 30, 33].

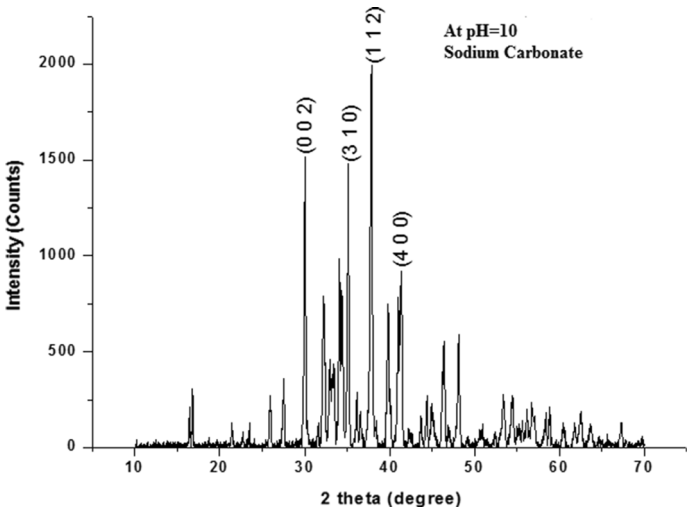

Fig. 6 XRD analysis of sodium carbonate

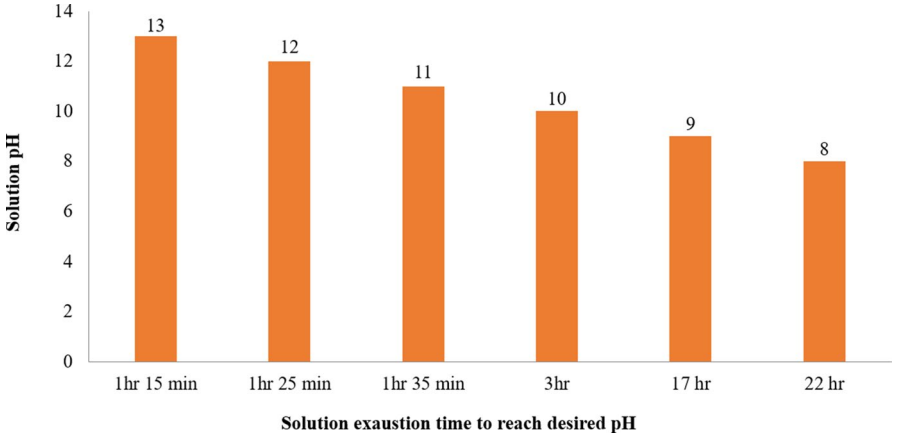

Fig. 7 Three Normal (3 N) sodium hydroxide solution exhaustion time (hr = hour, min = minute) to reach a different solution pH from the initial value. The solution starting pH was 13.75 at time $t = 0$ s

Nickel ferrite analysis

Nickel ferrite catalyst produced was used in the hydrogenation reaction of sodium hydrogen carbonate. Figure 8 shows the XRD results of the catalyst produced. Various researchers have used XRD and SEM analyses to determine the molecular structure and morphology of nickel ferrite catalyst. XRD results of this work

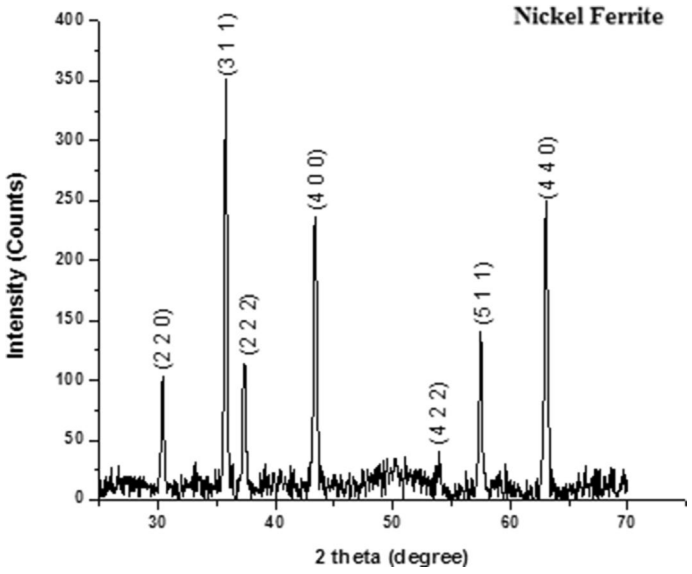

Fig. 8 XRD analysis of nickel ferrite

are in accordance with reported works of Silva et al. [34], Lin et al. [35] and Nejati et al. [36].

The sharp peaks in XRD analysis show the purity and crystalline structure of the catalyst produced.[37, 38]. MDI Jade 5.0 software analysis showed the dominating peaks obtained at 2θ, 30.3°, 35.7°, 37.3°, 43.3°, 53.8°, 57.3° and 62.9° which attribute to the plane (220), (311), (222), (400), (422), (511) and (440), respectively.

The SEM analysis of nickel ferrite revealed that the average particle size of the catalyst was 49.7 nm, which was well within the range earlier reported [37]. Figure 9 shows the spherical homogenous morphology of the nickel ferrite produced. Agglomeration was observed due to high energy dissipation and gases escape. The same agglomeration pattern was observed in the past study of Fu et al. [39] and Silva et al. [34].

Production of sodium formate

Sodium formate was produced from the hydrogenation of sodium hydrogen carbonate that was obtained at $pH = 8$ by the absorption of CO_2 in NaOH solution. The sodium formate synthesis reaction was carried out in the presence of nickel ferrite catalyst due to fact that nickel ferrite provides a medium for hydrogen carrier [40]. Besides, nickel ferrite has the surface property of decomposing CO_2, i.e., double bond of carbon with oxygen into a single bond between carbon and oxygen [41]. Thus, during hydrogenation of sodium hydrogen carbonate, CO_3^- is decomposed into CO_2 and sodium formate is formed as shown in Eq. 6 and Fig. 10.

$$NaHCO_3 + H_2 \xrightarrow{Ni(Fe_2O_4)} NaHCO_2 + H_2O \tag{6}$$

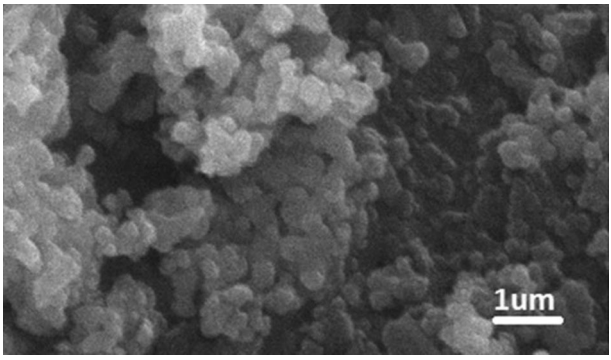

Fig. 9 SEM image of Nickel Ferrite catalyst

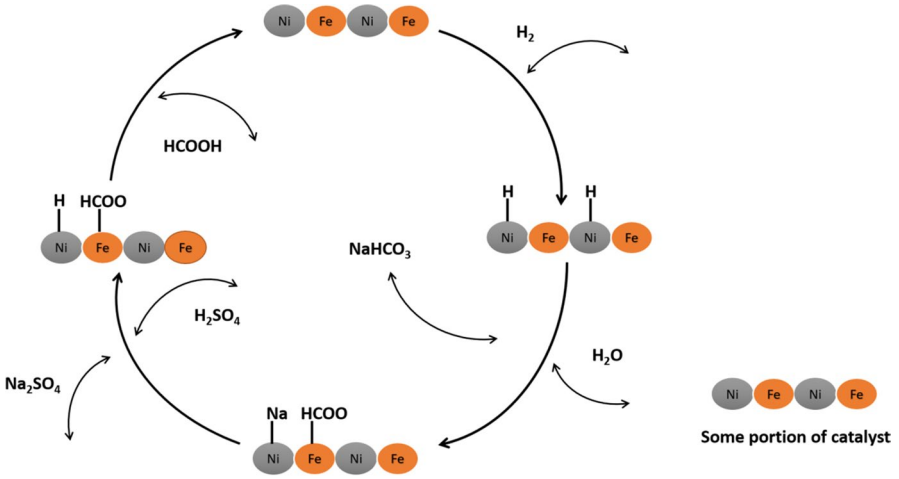

Fig. 10 Proposed overall mechanism of formic acid production by using a nickel ferrite catalyst

Synthesis and analysis of formic acid

The reaction of sodium formate produced with sulfuric acid showed a reaction %age yield of $79 \pm 0.2\%$. The proposed overall reaction mechanism of formic acid synthesis in this work from sodium hydrogen carbonate is shown in Fig. 10. The mechanism shows that hydrogen molecule comes in contact with Ni sites, and it dissociates into hydrogen atoms and adsorbed on Ni atoms. Further, oxygen molecules of $NaHCO_3$ are attracted toward Fe site and $HCOO^-$ anion produces and attached to Fe atoms. While Na^+ gets anchored with Ni sites by replacing the hydrogen. After that, another H atom from H_2SO_4 again makes the bond with Ni site replacing the Na^+. Finally, the formic acid is produced, as the surface of catalyst reduces. Similar kind of reaction findings are reported earlier for formic acid synthesis by using bimetallic catalysts [20, 23, 24].

For formic acid analysis, HPLC test was performed by running standard formic acid and its retention time was found to be 3.12 min. While the retention time of the produced formic acid is noted to be 3.10 min as shown in Fig. 11.

Formic acid from the reaction was separated upon vapor condensation using condensation assembly with round bottom flask. No formic acid was lost during the reaction as the decomposition of formic acid produces carbon monoxide only at very high temperatures of 1000° C and above [42, 43]. However, the temperature in current experimental work for formic acid vaporization only reached up to 100 ± 5° C. This resulted in the production of formic acid vapors only. Formic acid vapors produced were condensed continuously in the condenser assembly. In this study, the catalyst was not reused. Production of reaction by-product, sodium sulfate, further confirmed the reaction between the sulfuric acid and sodium formate. XRD analysis of sodium sulfate formed during the reaction is shown in Fig. 12. Sharp peaks of the product crystal were obtained at 2θ, 19.0°, 29.0°, 32.0° and 48.7° which correspond to the planes (111), (004), (131) and

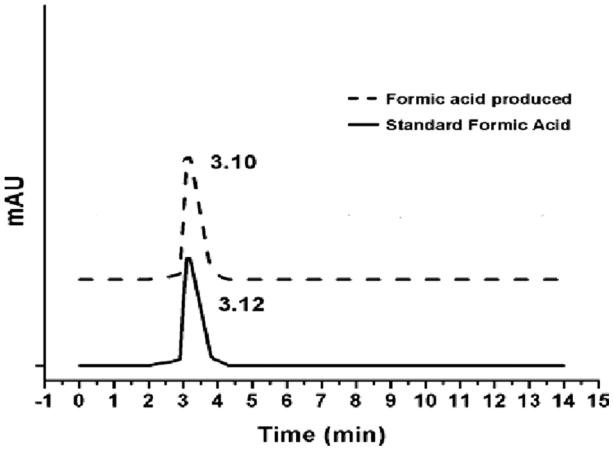

Fig. 11 HPLC analysis of formic acid

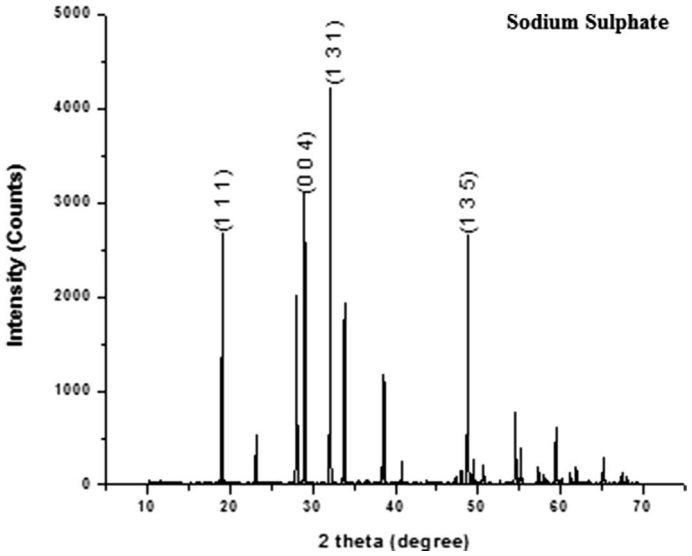

Fig. 12 XRD analysis of sodium sulfate

(135), respectively, confirming the crystal structure of sodium sulfate and the completion of the reaction.

Table 1 shows the comparison of catalyst used, operating temperature and %age yield of formic acid produced with this study. It shows that in this study, formic acid is produced at a lower temperature and a high %age yield is obtained as compared to previous works.

Table 1 Comparison of formic acid %age yield produced with literature. From CO_2 absorption and hydrogenation of the solution

S. no	Literature	Yield (%)	Temperature (°C)	Catalyst used	References
1	Chen et al. (2015)	50	300	$N_2H_4.H_2O$ over Ni catalyst	[21]
2	Wang et al. (2017)	86.6	200	Nonporous Ni catalyst	[22]
3	Chiang et al. (2018)	7.6	140	$Cu/ZnO/Al_2O_3$	[23]
4	Zhao et al. (2011)	35	50	Rhodium phosphine complex $[RhCl(mtppms)_3]$	[24]
5	Chiang et al. (2017)	13	140	$Cu/CuCr_2O_4$	[44]
6	Wu et al. (2009)	15.6	300	Ni as catalyst and Fe as a reductant Fe/Ni ratio 1:1	[45]
7	This Study	79 ± 0.2	80	Nickel ferrite catalyst ($NiFe_2O_4$)	Current work

Conclusions

The absorption of CO_2 and the time of exhaustion of the sodium hydroxide solution increase with an increase in the strength of sodium hydroxide solution and decreasing pH of the solution respectively. In addition, absorption reaction products are solution pH dependent. At solution pH 10, sodium carbonate is formed, and at pH 8, sodium hydrogen carbonate is formed while pH 9 gives Trona. Hydrogenation of sodium hydrogen carbonate in the presence of nickel ferrite catalyst produces sodium formate that is a precursor for formic acid synthesis. The hydrogenation process is endothermic. In the present study, addition of nickel ferrite catalyst lowered the hydrogenation temperature up to 80° C. The formic acid was synthesized from the sodium formate by the reaction with sulfuric acid. The %age yield of formic acid produced was noted $79 \pm 0.2\%$. The produced formic acid qualitative analysis by HPLC proved its production in the reaction. Further, XRD analysis confirmed the reaction by-product sodium sulfate formation. This work has shown that the value-added marketable products can be synthesized from the absorption of the pollutant gas CO_2 into the sodium hydroxide solution.

Acknowledgements The authors would like to acknowledge research funds provided by the School of Civil and Environmental Engineering, National University of Sciences and Technology, Islamabad, Pakistan.

Compliance with ethical standards

Conflict of interest The authors find no conflicts of interest in this work.

Geolocation information The reported work has been carried out in Islamabad, Pakistan.

References

1. F. Perera, Int. J. Environ. Res. Public. Health. **15**, 1 (2017)
2. R. Bindlish, Comput. Chem. Eng. **114**, 221 (2018)
3. S. Chu, Y. Cui, N. Liu, Nat. Mater. **16**, 16 (2016)
4. S. Chan, H. Asselt, T. Hale, K.W. Abbott, M. Beisheim, M. Hoffmann, B. Guy, N. Höhne, A. Hsu, P. Pattberg, P. Pauw, C. Ramstein, O. Widerberg, Glob. Policy. **6**, 466 (2015)
5. Intergovernmental Panel on Climate Change (IPCC), in Climate Change 2013: The physical science basis. contribution of working group I to the fifth assessment report of the intergovernmental panel on climate change ed. T.F. Stocker, D. Qin, G.-K. Plattner, M.M.B. Tignor, S.K. Allen, J. Boschung, A. Nauels, Y. Xia, V. Bex and P.M. Midgley (United Kingdom and New York, NY, USA., 2013)
6. S.R. Rintoul, S.L. Chown, R.M. DeConto, M.H. England, H.A. Fricker, V. Masson-Delmotte, T.R. Naish, M.J. Siegert, J.C. Xavier, Nature **558**, 233 (2018)
7. S. Kumar, R.K. Yadav, K. Ram, A. Aguiar, J. Koh, A.J.F.N. Sobral, J. CO2Util. **27**, 107 (2018)
8. G. Centi, S. Perathoner, Greenhouse Gases Sci. Technol. **1**, 21 (2011)
9. Z. Sun, R. Feng, L. Zhang, H. Xie, Res. Chem. Intermed. **44**, 3613 (2018)
10. D.H. Kim, Y.S. Ko, Res. Chem. Intermed. **44**, 3661 (2018)
11. V. Paolini, M. Torre, W. Giacopini, M. Pastori, M. Segreto, L. Tomassetti, M. Carnevale, F. Gallucci, F. Petracchini, E. Guerriero, Int. J. Greenhouse Gas Control. **83**, 186 (2019)
12. M.O. Vieira, W.F. Monteiro, B.S. Neto, V.V. Chaban, R. Ligabue, S. Einloft, React. Kinet. Mech. Catal. **126**, 987 (2019)
13. Y. Bian, S. Shen, Chin. J. Chem. Eng. **26**, 2318 (2018)
14. H.K. Karlsson, M.G. Sanku, H. Svensson, Int. J. Greenhouse Gas Control. **95**, 102952 (2020)
15. Y. Tavan, S.H. Hosseini, Petroleum. **3**, 51 (2017)
16. S.W. Kim, S.K. Behera, Y. Jamal, H.S. Park, J. Environ. Eng. **142**, C4015009 (2016)
17. A. Baltar, D. Gómez-Díaz, J.M. Navaza, A. Rumbo, AIChE J. **66**, e16770 (2020)
18. F. Christopher, J. Ralf, B. Albert, L. Gabor, B. Matthias, Chemsuschem **3**, 1048 (2010)
19. N. Bashiri, S.J. Royaee, M. Sohrabi, Res. Chem. Intermed. **44**, 217 (2018)
20. M. Wang, J. Zhang, N. Yan, Front. Chem. **1**, 17 (2013)
21. F. Chen, G. Yao, Z. Huo, F. Jin, RSC Adv. **5**, 11257 (2015)
22. T. Wang, D. Ren, Z. Huo, Z. Song, F. Jin, M. Chen, L. Chen, Green Chem. **19**, 716 (2017)
23. C.-L. Chiang, K.-S. Lin, H.-W. Chuang, J. Clean. Prod. **172**, 1957 (2018)
24. G. Zhao, F. Joó, Catal. Commun. **14**, 74 (2011)
25. M.A.H. Azizi, W.N.R.W. Isahak, M.S. Masdar, M.R. Somalu, M.A. Yarmo, Res. Chem. Intermed. **44**, 6787 (2018)
26. H. Zheng, N. Narkhede, L. Han, H. Zhang, Z. Li, Res. Chem. Intermed. **46**, 1749 (2020)
27. A.S. Goharrizi, B. Abolpour, Res. Chem. Intermed. **38**, 1389 (2012)
28. M. Yoo, S.-J. Han, J.-H. Wee, J. Environ. Manag. **114**, 512 (2013)
29. G. Yincheng, N. Zhenqi, L. Wenyi, Energy Procedia. **4**, 512 (2011)
30. M. Krauβ, R. Rzehak, Chem. Eng. Sci. **166**, 193 (2017)
31. C.-C. Lin, C.-R. Chu, Int. J. Greenhouse Gas Control. **42**, 117 (2015)
32. D. Darmana, R.L.B. Henket, N.G. Deen, J.A.M. Kuipers, Chem. Eng. Sci. **62**, 2556 (2007)
33. C. Fleischer, S. Becker, G. Eigenberger, Chem. Eng. Sci. **51**, 1715 (1996)
34. I.B.T. da Silva, A.G. D'Assunção, J.B.L. de Oliveira, S.M. de Holanda, Mater. Lett. **254**, 13 (2019)
35. K.-S. Lin, A.K. Adhikari, Z.-Y. Tsai, Y.-P. Chen, T.-T. Chien, H.-B. Tsai, Catal. Today. **174**, 88 (2011)
36. K. Nejati, R. Zabihi, Chem Cent J. **6**, 23 (2012)
37. Y.-J. Sun, Y.-F. Diao, H.-G. Wang, G. Chen, M. Zhang, M. Guo, Ceram. Int. **43**, 16474 (2017)
38. K. Maaz, S. Karim, A. Mashiatullah, J. Liu, M. Hou, Y. Sun, J. Duan, H. Yao, D. Mo, Y. Chen, Phys. B. **404**, 3947 (2009)
39. F. Yen-Pei, H. Chin-Shang, T. Kok-Wan, Jpn. J. Appl. Phys. **44**, 1254 (2005)
40. A. Goyal, S. Bansal, S. Singhal, Int. J. Hydrog. Energy. **39**, 4895 (2014)
41. H.-C. Shin, S.-C. Choi, K.-D. Jung, S.-H. Han, Chem. Mater. **13**, 1238 (2001)
42. D.S.Y. Hsu, W.M. Shaub, M. Blackburn, M.C. Lin, Symp. (Int.) Combust. **19**, 89 (1982)
43. D.A. Bulushev, J.R.H. Ross, Chemsuschem **11**, 821 (2018)

44. C.-L. Chiang, K.-S. Lin, H.-W. Chuang, C.-M. Wu, Int. J. Hydrog. Energy. **42**, 23647 (2017)
45. B. Wu, Y. Gao, F. Jin, J. Cao, Y. Du, Y. Zhang, Catal. Today. **148**, 405 (2009)